

Thanks for Nothing: Predicting Zero-Valued Activations with Lightweight Convolutional Neural Networks

Gil Shomron¹ Ron Banner² Moran Shkolnik^{1,2} Uri Weiser¹
Technion — Israel Institute of Technology¹
Intel — Artificial Intelligence Products Group (AIPG)²

{gilsho@tx, uri.weiser@ee}.technion.ac.il {ron.banner, moran.shkolnik}@intel.com

Abstract

Convolutional neural networks (CNNs) introduce state-of-the-art results for various tasks with the price of high computational demands. Inspired by the observation that spatial correlation exists in CNN output feature maps (ofms), we propose a method to dynamically predict whether ofm activations are zero-valued or not according to their neighboring activation values, thereby avoiding zero-valued activations and reducing the number of convolution operations. We implement the zero activation predictor (ZAP) with a lightweight CNN, which imposes negligible overheads and is easy to train and deploy on existing models. Furthermore, without model retraining, the same ZAP can be tuned to many different operating points along the accuracy-savings trade-off curve. For example, using VGG-16 and the ILSVRC-2012 dataset, two different operating points achieve a reduction of 20% and 30% multiply-accumulate (MAC) operations with top-1/top-5 accuracy degradation of 0.1%/0.04% and 1.3%/0.7% without fine-tuning of the entire model, respectively. Considering one-epoch fine-tuning, 45% MAC operations may be reduced with 1.3%/0.7% accuracy degradation.

1. Introduction

In the past decade, convolutional neural networks (CNNs) have been adopted for numerous applications [40, 37, 26], introducing state-of-the-art results. Despite being widely used, CNNs involve a considerable amount of computations. For example, classification of a 224x224 colored image requires billions of multiply-accumulate (MAC) operations [3, 43]. Such computational loads have many implications, from execution time to power and energy consumption of the underlying hardware.

CNN output feature maps (ofms) have been observed to exhibit spatial correlation, *i.e.*, adjacent ofm activations share close values [32, 39]. This observation is particularly

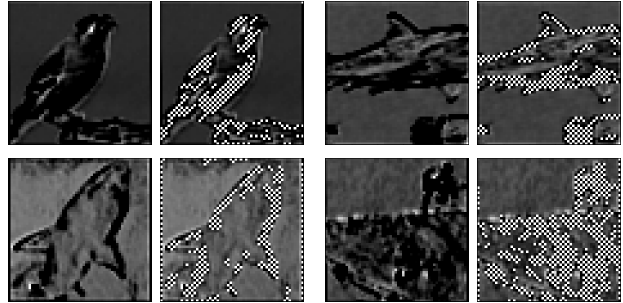


Figure 1: Exploiting spatial correlation for zero-value prediction of ofm activations with CNN-based predictor. Bright white pixels represent a predicted zero-valued ofm activation.

true for zero-valued activations, as it is common practice to use the ReLU activation function [33], which squeezes all negative values to zero. If it were possible to predict which of the convolution operations will result in a negative value, they could be skipped, their corresponding ofm activations could be set to zero, and many multiply-accumulate (MAC) operations could be saved.

Prediction mechanisms are at the heart of many general-purpose processors (GPPs), leveraging unique application characteristics, such as code semantics and temporal locality, to predict branch prediction outcomes and future memory accesses, for example. Prediction mechanisms may similarly be employed for CNNs. In this paper, we propose a prediction method for CNNs that dynamically classifies ofm activations as zero-valued or non-zero-valued by leveraging the spatial correlation of ofms. The zero activation predictor (ZAP) works in three-steps: first, only a portion of the ofm is fully computed; then, the remaining activations are classified as zero-valued or non-zero-valued using a lightweight convolutional neural network; and finally, the predicted non-zero-valued activations are computed while the zero-valued activations are skipped, thereby saving entire convolution operations (Figure 1). ZAP imposes neg-

ligible overheads in terms of computations and memory footprint, it may be plugged into pretrained models, and is trained quickly and in parallel. In addition, ZAP’s speculation level is tunable, enabling different operating options according to existing constraints.

ZAP may be considered a dynamic, unstructured, and magnitude-based ofm activations pruning strategy. Pruning typically includes two stages: network trimming and re-training. First, weights [12, 28] and activations [29, 14] are classified as insignificant according to some criterion and are discarded, followed by retraining phases to recoup the loss in accuracy. Increased model sparsity, when accompanied with the appropriate hardware [2, 11, 34, 38], leads to a decrease in MAC operations. Since our method focuses strictly on the zero-valued ofm activations, ZAP can capture a range of operation points that does not require re-training. That said, ZAP is also capable of pruning when set to high speculation levels, as more mispredictions of non-zero-valued activations as zero-valued activations take place. Interestingly, we observe that these mispredictions usually occur with small activation values, which is practically a magnitude-based pruning strategy.

This paper makes the following contributions:

- **Zero activation predictor (ZAP).** We introduce a dynamic, easy to deploy, CNN-based zero-value prediction method that exploits the spatial correlation of output feature map activations. Compared with conventional convolution layers, our method imposes negligible overheads in terms of both computations and parameters.
- **Trade-off control.** We estimate the model’s entire accuracy-to-savings trade-off curve with mostly local statistics gathered by each predictor. This provides a projection of the model and the predictor performance for any operating point.
- **Accuracy to error linearity.** We show, both analytically and empirically, that the entire model accuracy is linear with the sum of local misprediction errors, assuming they are sufficiently small.

2. ZAP: Zero Activation Predictor

In this section, we describe our prediction method and its savings potential. We analyze its overheads in terms of computational cost and memory footprint and show that both are negligible compared with conventional convolution layers.

2.1. Preliminary

A convolution layer consists of a triplet $\langle X_i, X_o, W \rangle$, where X_i and X_o correspond to the input and output activation tensors, respectively, and W corresponds to the set

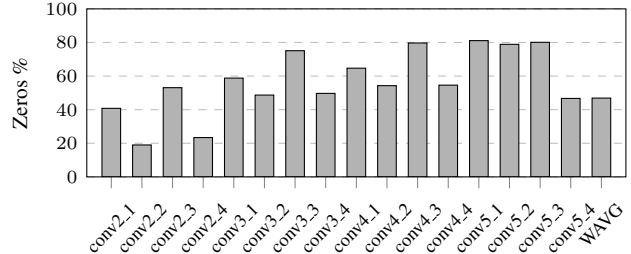


Figure 2: ResNet-18 ofm sparsity as measured across the entire ILSVRC-2012 validation set. Each bar represents the relative portion of zero-valued ofm activations within that same layer. Considering the different ofm dimensions, sparsity is 47%.

of convolution kernels. Each activation tensor is a three-dimensional tensor of size $w \times h \times c$, where w , h and c represent the tensor width, height, and depth, respectively. For convenience, the dimensions of X_i and X_o are denoted by $[w_i \times h_i \times c_i]$ and $[w_o \times h_o \times c_o]$. Finally, the set of convolution kernels W is denoted by a four-dimensional tensor $[k \times k \times c_i \times c_o]$, where k is the filter width and height. The filter width and height are not necessarily equal, but it is common practice in most conventional CNNs to take them a such. Given the above notations, each output activation value $X_o[x, y, z]$ is computed from the input tensor X_i and weights W as follows:

$$X_o(x, y, z) = \sum_{i,j=0}^{k-1} \sum_{c=0}^{c_i-1} X_i[x+i, y+j, c] \cdot W[i, j, c, z], \quad (1)$$

where the bias term is omitted for simplicity’s sake. We use the above notations throughout this paper.

2.2. Three-Step Method

Conventional convolution layers compute their ofm by applying Equation (1) for each $[x, y, z]$. It has been observed that ofms accommodate many zero-valued activations due to the widespread usage of the ReLU activation function. For example, in Figure 2 we present the relative portion of zero-valued activations of ResNet-18 [13] with the 2012 ImageNet large scale visual recognition challenge (ILSVRC-2012) dataset [36] — overall, almost 50% of the ofm activations are zero-valued; therefore, 50% of the MAC operations may be potentially skipped. Moreover, ofm activations exhibit spatial correlation [32, 39], meaning that a group of activation values testifies about other adjacent activation values.

We suggest a three-step dynamic prediction mechanism that locates zero-valued ofm activations by exploiting the spatial correlation inherent in CNNs to potentially skip them and reduce the computational burden of the model.

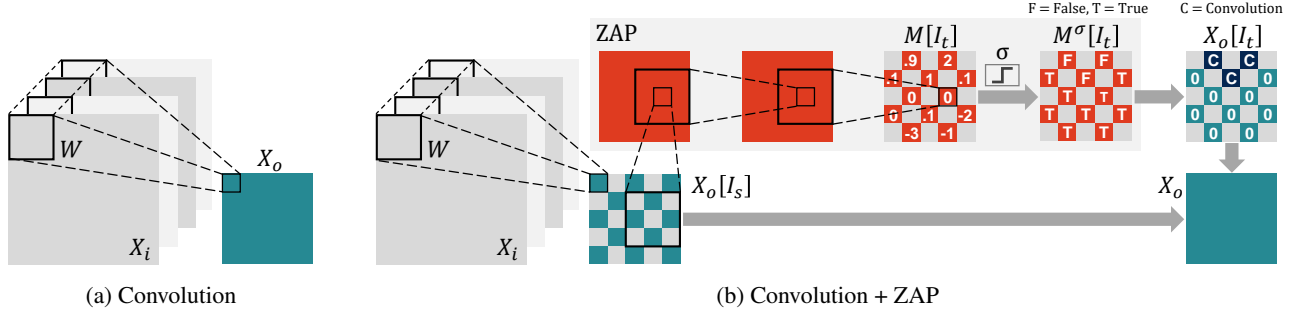


Figure 3: Illustration of a single ofm channel convolution without ZAP (a) and with ZAP (b). $X_o[I_s]$ is computed based on a pre-defined pattern. $X_o[I_s]$ is then subjected to ZAP, which produces a prediction map $M[I_t]$, followed by a thresholding step to form the binary prediction map $M^\sigma[I_t]$. $X_o[I_t]$ is created according to $M^\sigma[I_t]$ — a portion of the I_t ofm activations are predicted as zero-valued and skipped, whereas the rest are computed using Equation (1).

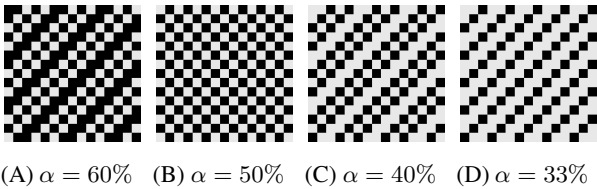


Figure 4: Partial ofm convolution patterns. Black pixels represent computed activations.

Given an ofm, X_o , we divide its indices into two subsets (I_s, I_t) according to a pre-defined pattern. Then, the following three steps are carried out (as illustrated in Figure 3): (i) the values that belong to indices I_s are fully computed in the conventional manner, resulting in a sparse ofm, $X_o[I_s]$; (ii) this partial ofm ($X_o[I_s]$) is passed through our predictor to yield a binary map, $M^\sigma[I_t]$, which is used to predict the zero values in $X_o[I_t]$; and (iii) all values predicted to be non-zero by $M^\sigma[I_t]$ are computed. We describe this process in detail next.

Computation pattern. $X_o[I_s]$ is computed based on a pre-defined pattern as depicted in Figure 4. We use α to denote the ratio between the number of activations computed in the partial ofm and the ofm dimensions. This may be formally formulated as $\alpha \equiv \frac{|I_s|}{w_o h_o c_o}$, where $|I_s|$ is the set cardinality.

By decreasing α , less ofm activations are computed prior to the prediction, which may potentially lead to the saving of more operations. For example, for $\alpha = 40\%$, 60% of the activations may potentially be saved. Less prior data about the ofm may, however, lead to higher misprediction rates, which in turn may decrease model accuracy.

Prediction process via lightweight CNN. Given the partial ofm, $X_o[I_s]$, our goal is to produce an output computation mask that predicts which of the remaining activations are zero-valued and may be skipped. Recall that ofm activa-

tions are originally computed using Equation (1) and so the prediction process must involve less MAC operations than the original convolution operation with as minimal memory footprint as possible.

We use a CNN to implement ZAP. We exploit the spatial correlation inherent in CNNs [32, 39, 21, 8] and use only depthwise convolution (DW-CONV) layers [16], *i.e.*, only spatial filters with no depth ($k \times k \times 1 \times c_o$). As such, we obtain a lightweight model in terms of both MAC operations and parameters (further analyzed in Section 2.3). Our CNN comprises a 3x3 DW-CONV layer followed by a batch normalization (BN) layer [20] followed by ReLU, twice. DW-CONV layer padding and stride are both defined as 1 to achieve equal dimensions throughout the CNN predictor. During training, the last ReLU is capped at 1 [23], whereas during inference we discard the last ReLU activation and use a threshold.

Thresholding. Although ZAP is trained to output a binary classifier (described in Section 4.1), ZAP naturally outputs $M[I_t]$, which is not a strict binary mask but rather a range of values that corresponds to a prediction confidence [10, 44] of whether the ofm activation is zero-valued or not. To binarize ZAP’s output, we define a threshold σ that sets the level of prediction confidence; therefore, $M^\sigma[I_t] = M[I_t] > \sigma$ (boolean operation).

According to $M^\sigma[I_t]$, part of the ofm activations in $X_o[I_t]$ are predicted to be non-zero-valued and are computed, whereas the others are predicted to be zero-valued and are skipped. When an ofm activation is predicted to be zero-valued, two types of misprediction may occur. First, an actual zero-valued activation may be predicted as a non-zero-valued activation and so redundant MAC operations may take place. Second, an actual non-zero-valued activation may be predicted as zero. The latter misprediction increases the model error, potentially decreasing model accuracy.

The motivation behind ZAP is clear — reducing compu-

tations by skipping convolution operations. Its impact on the model accuracy, number of computations, and amount of parameters has yet, however, to be discussed. We next discuss the overhead of ZAP, and in Section 4, we show empirically how ZAP affects the accuracy of different model architectures.

2.3. Overhead Analysis

ZAP is a CNN by itself, which means that it introduces additional computations and parameters. To be beneficial, it must execute less operations per ofm activation than the original convolution operation. A conventional convolution layer requires $k^2 c_i$ MAC operations per ofm activation. On the other hand, the number of MAC operations required by a two-layered DW-CONV ZAP for a single ofm activation is K^2 , where K is the filter width and height. Note that ZAP’s first layer needs only to consider $|I_s|$ values for computation since, according to the pre-defined pattern, the remaining $|I_t|$ values are zero; the second layer needs only to compute $|I_t|$ ofm activations.

Compared with a standard convolution operation, and for the case of $K = k$,

$$\frac{\text{ZAP ops.}}{\text{standard convolution ops.}} = \frac{1}{c_i}. \quad (2)$$

c_i is usually greater than 10^2 [13, 41, 25], in which case $1/c_i \approx 0$ and ZAP overhead is, therefore, negligible.

Regarding the parameters, a conventional convolution layer requires $k^2 c_i c_o$ parameters and a two-layered DW-CONV requires $2K^2 c_o$ parameters. Given c_i conventional sizes and $K = k$, ZAP’s memory footprint is negligible as well.

3. Trade-Off Control

The threshold hyperparameter, σ , represents the prediction confidence of whether an ofm activation is zero or non-zero. Users should, however, address the accuracy and MAC reduction terms rather than using σ , since it is not clear how a specific σ value affects accuracy and savings. In this section, we show that, given some statistics, we can estimate the entire model accuracy and predictor MAC savings, thereby avoiding the need to address the threshold value directly and providing the user with an accuracy-MAC savings trade-off control “knob”.

3.1. Accuracy, MAC Savings, and Threshold

Accuracy and threshold. Consider a DNN with L layers. Each layer i comprises weights w_i , an ifm x_i , and an ofm y_i . When predictions are avoided, layer $i + 1$ input, x_{i+1} , is given by

$$x_{i+1} = y_i = \max(x_i w_i, 0), \quad (3)$$

where $\max(\cdot, 0)$ is the ReLU activation function.

Our predictor is not perfect and may zero out non-zero elements with a small probability ε_i . Therefore, non-zero inputs to layer $i + 1$ have a probability ε_i of becoming zero and a probability $1 - \varepsilon$ of remaining y_i . Using y_i^π to denote the prediction of output y_i , we obtain the following error in the expected activation:

$$E(y_i^\pi) = (1 - \varepsilon_i) \cdot E(y_i). \quad (4)$$

In other words, the prediction at each layer i introduces a multiplicative error of $(1 - \varepsilon_i)$ with respect to the true activation. This multiplicative error builds up across layers. For an L -layer network, the expected network outputs are scaled down with respect to the true network outputs as follows:

$$\text{Scale Error} = \prod_{i=1}^L (1 - \varepsilon_i). \quad (5)$$

Note that for a sufficiently small ε , $1 - \varepsilon = e^{-\varepsilon}$. Therefore, assuming sufficiently small misprediction probabilities, $\{\varepsilon_i\}$, we obtain the following expression

$$\begin{aligned} \text{Scale Error} &= \prod_{i=1}^L (1 - \varepsilon_i) \approx \prod_{i=1}^L e^{-\varepsilon_i} \\ &= e^{-\sum_{i=1}^L \varepsilon_i} \approx 1 - \sum_{i=1}^L \varepsilon_i, \end{aligned} \quad (6)$$

where the approximations can easily be extracted from a Taylor expansion to e^{-x} . Equation (6) shows that the final error due to small mispredictions accumulates along the network in a *linear* fashion when the errors due to mispredictions are small enough.

Denoting the output of layer i for a threshold σ by $y_i^{\pi, \sigma}$, the error is associated with a threshold σ as follows:

$$\begin{aligned} \text{Scale Error}(\sigma) &\approx 1 - \sum_{i=1}^L \varepsilon_i(\sigma) \\ &= 1 - \sum_{i=1}^L \left(1 - \frac{\sum_{x,y,z} y_i^{\pi, \sigma}[x, y, z]}{\sum_{x,y,z} y_i[x, y, z]} \right), \end{aligned} \quad (7)$$

where Equation (4) is used for the last transition. Figure 5 shows that this analytical observation is in good agreement with our empirical results.

Ideally, we would like to have a scale error that is as close as possible to 1 so as to avoid shifting the network statistics from the learned distribution. When the scale error is 1, network outputs remain unchanged and no accuracy degradation associated with mispredictions occurs. Yet, as σ increases, more ofm activations are predicted as zero-valued, decreasing the scale error below 1, as exhibited by Equation (7). This scale error decreases monotonically with σ

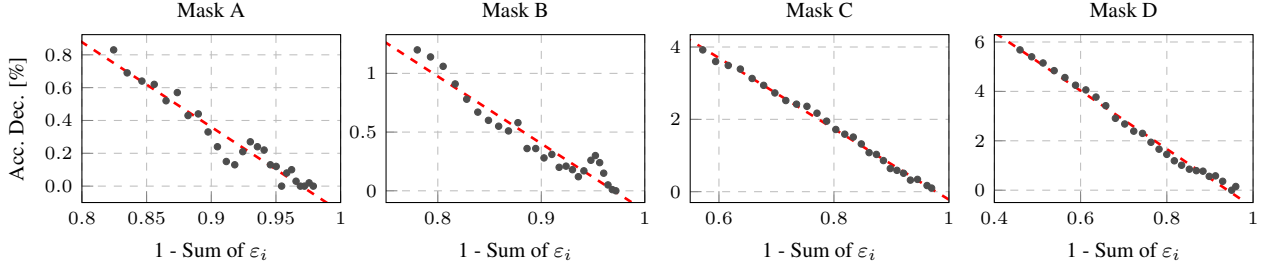


Figure 5: AlexNet + CIFAR-100 top-1 accuracy decrease as a function of $1 - \sum_{i=1}^L \varepsilon_i(\sigma)$. Each dot represents a measurement with a different threshold: the leftmost and rightmost thresholds are 0 and 0.5, respectively. Measurements were taken in steps of 0.02.

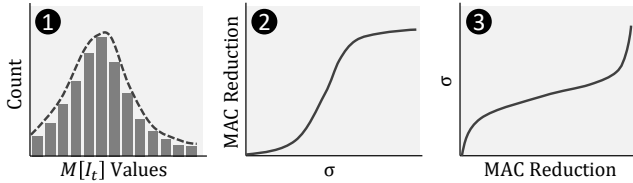


Figure 6: The transformation process from a prediction values histogram (or distribution) to the threshold versus MAC reduction curve.

and introduces an inverse mapping, which enables us to define a threshold value for any desired accuracy degradation.

At this point, given the model accuracy-error linearity and the error to threshold transformation, we have a transformation from accuracy to threshold and vice versa. Next, we discuss the relationship between MAC savings and σ .

MAC savings and threshold. Recall that $M[I_t]$ represents the collection of values predicted by ZAP for a given layer before applying the threshold. For readability, assume $m(x)$ is the probability density function of $M[I_t]$ values (*i.e.*, continuous). Then, the number of ofm activations predicted as zeros relative to I_t can be expressed as follows:

$$\text{Zero Prediction Rate } (\sigma) = \int_{-\infty}^{\sigma} m(x) dx. \quad (8)$$

To achieve the actual MAC reduction in layer i , the layer dimensions, α , and ZAP overhead should be considered. Clearly, the total MAC reduction equals the sum of the contributions from all layers. Note that the zero prediction rate, and therefore the MAC reduction, increases monotonically, and for a certain range it may be considered a strictly monotonic function. Inverse mapping from MAC reduction to σ is, therefore, possible, as depicted in Figure 6.

Putting it all together. Given the derivations so far, it is possible to make an *a priori* choice of any operating point, given estimates about the desired accuracy and MAC reduction, without directly dealing with the threshold. Assume a pre-processing step that consists of collecting statistical

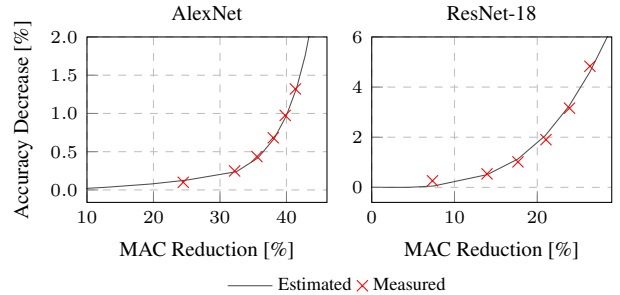


Figure 7: Estimated top-5 accuracy-MAC savings trade-off curve using mask B and ILSVRC-2012 dataset. The measured operating points correspond to thresholds of 0 to 0.5, in steps of 0.1.

information about the prediction values $M[I_t]$ and at least two accuracy measurements of the entire model, to obtain the linear accuracy-error relationship. With this statistical information, we can effectively estimate the desired operating point, as demonstrated in Figure 7.

3.2. Non-Uniform Threshold

Thus far, for the sake of simplicity, σ was set uniformly across all layers. Layers, however, behave differently, and so ZAP error and savings may differ between layers for a given threshold. This is evident in Figure 8 in which we present the error and total MAC operations of four layers in ResNet-18. Notice how the error of layer 6 (L6) increases earlier than the other layers, for example. Ideally, given L layers, we would like to choose a threshold per layer, σ_i , to save as many MAC operations as possible, given an error (or accuracy) constraint, ϵ , *i.e.*,

$$\begin{aligned} & \text{minimize} && \sum_{i=1}^L \text{MAC ops}_{\cdot i}(\sigma_i) \\ & \text{subject to} && \sum_{i=1}^L \varepsilon_i(\sigma_i) \leq \epsilon \propto \text{Accuracy}. \end{aligned} \quad (9)$$

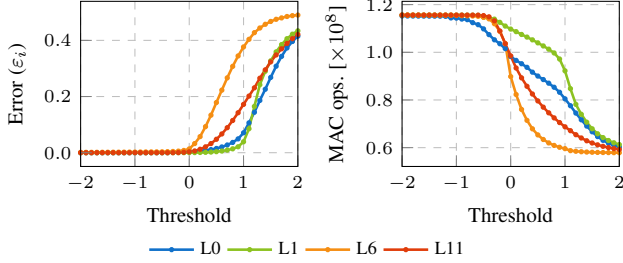


Figure 8: ResNet-18 + ILSVRC-2012 example of different layers behavior in terms of error and MAC operations as a function of ZAP threshold.

We use curve fitting to define a parameterized sigmoid function for the error and for the MAC operations of each layer and apply standard non-linear optimization methods to solve Equation (9) (see supplementary material for curve fitting results). It is worth mentioning that Equation (9) can also be written the other way around, that is, minimizing the error given a computation budget.

4. Experiments

In this section, we evaluate ZAP performance in terms of MAC savings and accuracy degradation using various model architectures and datasets, and compare our results to previous work.

4.1. ZAP Training

ZAPs are deployed at each desired convolution layer and are trained independently. By training in isolation [14, 7], ZAPs can be plugged into a model without altering its architecture and trained parameters and may be trained in parallel. First, a batch is fed forward bypassing all predictors. During the feedforward phase, each ZAP saves a copy of its local input feature map (ifm) and corresponding local ofm. Then, each ZAP computes its $M[I_t]$, using its ifm followed by a ReLU activation function which is capped at 1. The ground truth, M_{ideal} , of each ZAP is its local ofm passed through a zero-threshold boolean operation at indices I_t . Finally, the MSE loss is used to minimize each of the predictor errors, as follows:

$$\min \sum_{(x,y,z) \in I_t} (M - M_{ideal})^2. \quad (10)$$

ZAP training is illustrated in Figure 9.

4.2. Experimental Setup

We evaluated our method using CIFAR-100 [24] and ILSVRC-2012 [36] datasets, and AlexNet [25], VGG-16 [41], and ResNet-18 [13] CNN architectures. The source

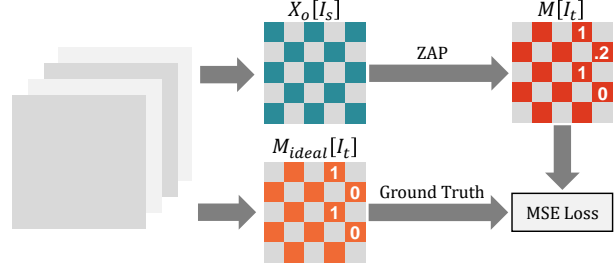


Figure 9: Illustration of the training of a single ZAP. The ground truth is the original layer ofm after a binary threshold operation (>0). The CNN predictor is used with the ReLU activation function capped at 1.

code is publicly available¹.

ZAPs were trained using the Adam [22] optimizer for 5 epochs. When the ILSVRC-2012 dataset was used for ZAPs training, only 32K training set images were used. After ZAPs were trained, we recalibrated the running mean and variance of the model BN layers; this is not considered fine-tuning since it does not involve backpropagation. BN recalibration was noticeably important with ResNet-18, which has multiple BN layers. When fine-tuning was considered, it was limited to 5 epochs with CIFAR-100 and to 1 epoch with ILSVRC-2012. We did not deploy ZAPs on the first layers of any of the models, since it is not beneficial in terms of potential operation savings.

AlexNet with CIFAR-100 was trained from scratch using the original hyperparameters, achieving top-1 accuracy of 64.4%. AlexNet, VGG-16, and ResNet-18 with ILSVRC-2012 were used with the PyTorch pretrained parameters, achieving top-1/top-5 accuracies of 56.5%/79.1%, 71.6%/90.6%, and 69.8%/89.1%, respectively.

We experimented with four different prediction patterns (Figure 4). The same prediction pattern was used across all layers and channels. Mixing patterns in layer and channel granularity is an option we leave for future work.

Throughout this section, MAC reduction is defined as $(1 - \text{after}/\text{before})$ and accuracy degradation is defined as $(\text{before} - \text{after})$. When discussing MAC reduction, we consider only the relative savings from convolution layers.

4.3. CIFAR-100

Operating points. We demonstrate different operating points as measured with different masks and uniform thresholds across all layers with AlexNet using the CIFAR-100 dataset. For each operating point, we report the entire model top-1 accuracy degradation and MAC operation savings, with and without fine-tuning (Figure 10). For example, considering a 1% top-1 accuracy degradation cap, ZAP achieves a 32.4% MAC reduction with 0.7% accuracy

¹<https://github.com/gilsh/zap>

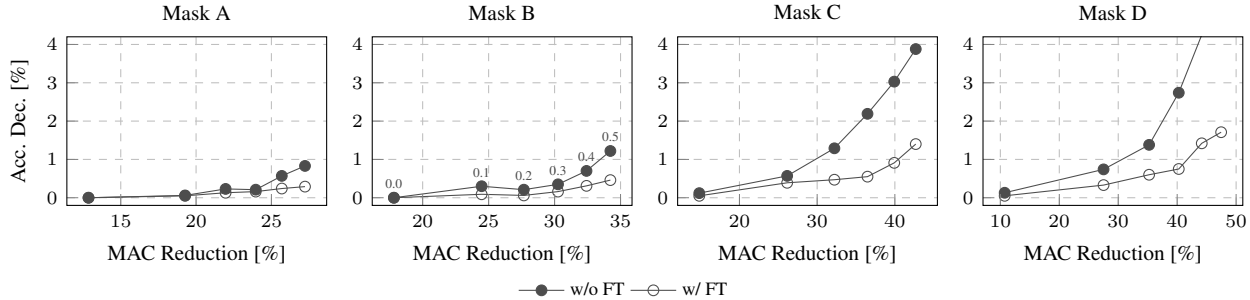


Figure 10: Demonstrating the different operating points of AlexNet + CIFAR-100 with (w/) and without (w/o) fine-tuning (FT). Accuracy measurements are top-1. Threshold range is set between 0 to 0.5, in steps of 0.1. Each measurement corresponds to a threshold, as presented in “Mask B” plot.

degradation at mask B with a 0.4 threshold. In addition, by fine-tuning the model, our predictor achieves 40.3% MAC reduction with 0.8% accuracy degradation at mask D with a 0.3 threshold.

Masks with greater α values lead to ofms with relatively more computed activations, *i.e.*, larger $|I_s|$. We observe that these masks show better accuracy results in the low degradation region (*e.g.*, mask A versus mask D at 20% MAC reduction), whereas for higher MAC reduction requirements, masks with lower α values are preferred. In order to achieve high MAC reductions with the former masks (for example, mask A), σ would have to be cranked up. Since the prediction potential of these masks is low to begin with (for example, the best-case scenario with mask A is 40% activations savings with mask A), high thresholds will lead to pruning of relatively significant values and, as a result, to significant accuracy degradation. On the other hand, for conservative MAC reductions, these masks are preferred, since their speculation levels are lower and prediction confidence is higher.

Misprediction breakdown. The model accuracy is not solely dependent on *how many* non-zeros were predicted as zero, but also *which* values were zeroed out. The notion that small values within DNN are relatively ineffectual is at the core of many pruning techniques. In Figure 11 we present the mispredicted activation values distribution, normalized to the number of ofm activations for value steps of 0.1. For example, when using $\sigma = 0$, 0.15% of ofm activations with original values between 0 to 0.1 were zeroed out. Increasing the threshold level increases the number of predicted and mispredicted ofm activations. It is apparent that insignificant values are more prone to be mispredicted — it is easier to be mistaken about zeroing out a small value than a large value — attesting to the correlation between σ and the prediction confidence level.

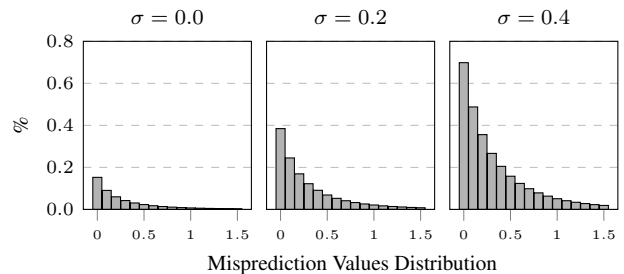


Figure 11: AlexNet + CIFAR-100 histograms of non-zero values that were predicted as zero using mask B and different uniform thresholds.

4.4. ILSVRC-2012

Comparison with previous work. In Table 1 we compare our method with the work of Figurnov *et al.* [8], Kim *et al.* [21], Shomron and Weiser [39], and Dong *et al.* [6]. Thresholds are set by solving Equation 9. Using AlexNet and VGG-16, our method shows better results across the board (besides a small difference of 0.07 with VGG-16 top5 compared to Kim *et al.*) — for more MAC savings, a smaller accuracy drop is observed. Regrading ResNet-18, our method shows better results compared with Shomron and Weiser but falls short when compared with Dong *et al.* Notice though that the method Dong *et al.* introduced involves an entire network training with *hundreds* of epochs. Therefore, even though there is some resemblance between our method and theirs, the results themselves are not necessarily comparable.

5. Related Work

Speculative execution. GPPs make extensive use of speculative execution of actions [15]. For example, branch predictors are used to predict whether a branch instruction will be taken (or not taken) based on previous encounters with that branch or other nearby branches, and caches are

Network	Paper	Related Work					Ours				
		Top1	Top1-ft	Top5	Top5-ft	MAC	Top1	Top1-ft	Top5	Top5-ft	MAC
AlexNet	Figurnov <i>et al.</i>	-	-	8.50	2.0	50.0%	4.63	1.97	3.04	1.17	51.1%
	Kim <i>et al.</i>	0.48	-	0.40	-	28.6%	0.34	0.33	0.24	0.14	32.4%
	Shomron and Weiser	4.00	1.6	2.90	1.3	37.8%	1.28	0.78	0.84	0.42	38.0%
VGG-16	Figurnov <i>et al.</i>	-	-	15.6	1.1	44.4%	11.02	1.27	7.02	0.71	44.5%
	Kim <i>et al.</i>	0.68	-	0.26	-	25.7%	0.54	0.24	0.33	0.11	26.2%
	Shomron and Weiser	3.60	0.7	2.00	0.4	30.7%	1.71	0.31	0.87	0.19	31.3%
ResNet-18	Dong <i>et al.</i> *	-	3.6	-	2.3	34.6%	12.35	7.22	8.37	4.66	34.0%
	Shomron and Weiser	11.0	2.7	7.60	1.7	22.7%	2.96	1.86	1.70	1.13	23.8%

Table 1: MAC reduction and accuracy with and without fine-tuning (ft) — our results compared with previous work. The accuracy columns represent the decrease in accuracy. The MAC columns represent the MAC operations reduction. The minus (‘-’) symbol represents unpublished data. See supplementary material for execution details.

used to store values that will probably be accessed repetitively in the near future. These speculative mechanisms leverage unique application characteristics, such as code semantics and temporal locality, to better utilize the GPP’s internal structure to achieve better performance.

Researchers have also studied the speculative execution of CNNs to decrease their compute demands. Akhlaghi *et al.* [1] predict during the convolution computation whether the convolution results will end up negative. Song *et al.* [42], Lin *et al.* [30], and Chang *et al.* [4] predict whether an entire convolution result is negative according to a partial result yielded by the input MSB bits. Huan *et al.* [19] avoid convolution multiplications by predicting and skipping near-zero valued data, given certain thresholds. Chen *et al.* [5] predict future weight updates during training based on Momentum [35] parameters. Zhu *et al.* [45] use a fully connected layer to predict each ofm activation sign and low-rank approximation to decrease the weight matrix.

In conventional GPPs, control and data mispredictions may lead to a pipeline flush and a rewind of the program counter, *i.e.*, it is common that an execution stops and starts over due to mispredictions. Interestingly, this is not the case with DNNs, since they are statistics-based and tolerant to errors (to some extent) [27]. Therefore, the impact of mispredictions on the model accuracy depends on *how many* non-zero-valued activations are predicted as zero, as well as on *which* values were zeroed out.

Spatial correlation. The correlation between neighboring activations in CNN feature maps is an inherent CNN characteristic that may be exploited. Shomron and Weiser [39], Kim *et al.* [21], and Figurnov *et al.* [8] partially compute the ofmap activations and interpolate the rest. Shomron and Weiser, and Kim *et al.* focus on predicting zero-valued activations whereas Figurnov *et al.* mainly use “nearest neighbor” to interpolate missing values. Finally, Mahmoud *et al.* [32] operate on reduced precision deltas between adjacent activations rather than on true values.

Dynamic pruning. As opposed to static pruning [12, 17,

31, 31, 28], dynamic pruning is input-dependent. Dong *et al.* [6] present a network structure with embedded low-cost convolution layers that act as zero-valued activation masks for the original convolution masks. In a higher granularity, Lin *et al.* [29] use reinforcement learning for channel pruning, Hua *et al.* [18] use a network structure with embedded channel gating capability, Gao *et al.* [9] prune channels according to a channel saliency map followed by a fully connected layer, and He *et al.* [14] propose a two-step channel pruning algorithm with LASSO regression and fine-tuning of weights. All these works, except [14], involve extensive model training.

Our work is most closely related to the work of Dong *et al.*, Shomron and Weiser, Kim *et al.*, and Figurnov *et al.*, with which we have also compared our results. However, our work provides the user with a continuous range of operating points and offers a prior estimate of the model accuracy degradation and MAC savings. Specifically, in contrast to Dong *et al.*, our approach is easy to deploy (fine-tuning of the entire model, at most) and relies on partial ofm computation rather than on the ifm. As for Shomron and Weiser, Kim *et al.*, and Figurnov *et al.*, we create the binary prediction masks using a CNN-based approach.

6. Conclusions

We propose a zero activation predictor (ZAP) that dynamically identifies the zero-valued output feature map (ofm) activations prior to their computation, thereby saving their convolution operations. ZAP exploits the spatial correlation of ofm activations inherent in convolution neural networks, meaning that according to a sparsely computed ofm, ZAP determines whether the remaining activations are zero-valued or non-zero-valued. ZAP is a lightweight CNN that imposes negligible computation and parameter overheads and its deployment and training does not require a modification of the baseline model architecture and parameters. In addition, ZAP speculation level is tunable, allowing an efficient *a priori* control of its accuracy-savings trade-off.

Acknowledgments

We gratefully acknowledge the support of NVIDIA Corporation and its donation of the Titan V GPU used for this research.

References

- [1] Vahideh Akhlaghi, Amir Yazdanbakhsh, Kambiz Samadi, Rajesh K Gupta, and Hadi Esmailzadeh. SnaPEA: Predictive early activation for reducing computation in deep convolutional neural networks. In *International Symposium on Computer Architecture (ISCA)*, pages 662–673. IEEE, 2018.
- [2] Jorge Albericio, Patrick Judd, Tayler Hetherington, Tor Aamodt, Natalie Enright Jerger, and Andreas Moshovos. Cnvlutin: Ineffectual-neuron-free deep neural network computing. In *International Symposium on Computer Architecture (ISCA)*, pages 1–13. IEEE, 2016.
- [3] Alfredo Canziani, Adam Paszke, and Eugenio Culurciello. An analysis of deep neural network models for practical applications. *arXiv preprint arXiv:1605.07678*, 2016.
- [4] Jiho Chang, Yoonsung Choi, Taegyong Lee, and Junhee Cho. Reducing MAC operation in convolutional neural network with sign prediction. In *International Conference on Information and Communication Technology Convergence (ICTC)*, pages 177–182. IEEE, 2018.
- [5] Chi-Chung Chen, Chia-Lin Yang, and Hsiang-Yun Cheng. Efficient and robust parallel dnn training through model parallelism on multi-gpu platform. *arXiv preprint arXiv:1809.02839*, 2018.
- [6] Xuanyi Dong, Junshi Huang, Yi Yang, and Shuicheng Yan. More is less: A more complicated network with less inference complexity. In *Conference on Computer Vision and Pattern Recognition (CVPR)*, pages 5840–5848. IEEE, 2017.
- [7] Ahmed T Elthakeb, Prannoy Pilligundla, and Hadi Esmailzadeh. Divide and conquer: Leveraging intermediate feature representations for quantized training of neural networks. *International Conference on Machine Learning (ICML) Workshop on Understanding and Improving Generalization in Deep Learning*, 2019.
- [8] Mikhail Figurnov, Aizhan Ibrahimova, Dmitry P Vetrov, and Pushmeet Kohli. PerforatedCNNs: Acceleration through elimination of redundant convolutions. In *Advances in Neural Information Processing Systems (NIPS)*, pages 947–955, 2016.
- [9] Xitong Gao, Yiren Zhao, Lukasz Dudziak, Robert Mullins, and Cheng-zhong Xu. Dynamic channel pruning: Feature boosting and suppression. *International Conference on Learning Representations (ICLR)*, 2018.
- [10] Yonatan Geifman and Ran El-Yaniv. Selective classification for deep neural networks. In *Advances in Neural Information Processing Systems (NIPS)*, pages 4878–4887, 2017.
- [11] Song Han, Xingyu Liu, Huizi Mao, Jing Pu, Ardavan Pedram, Mark A Horowitz, and William J Dally. EIE: efficient inference engine on compressed deep neural network. In *International Symposium on Computer Architecture (ISCA)*, pages 243–254. IEEE, 2016.
- [12] Song Han, Huizi Mao, and William J Dally. Deep compression: Compressing deep neural networks with pruning, trained quantization and huffman coding. In *International Conference on Learning Representations (ICLR)*, 2016.
- [13] Kaiming He, Xiangyu Zhang, Shaoqing Ren, and Jian Sun. Deep residual learning for image recognition. In *Conference on Computer Vision and Pattern Recognition (CVPR)*, pages 770–778. IEEE, 2016.
- [14] Yihui He, Xiangyu Zhang, and Jian Sun. Channel pruning for accelerating very deep neural networks. In *International Conference on Computer Vision (ICCV)*, pages 1389–1397. IEEE, 2017.
- [15] John L Hennessy and David A Patterson. *Computer architecture: a quantitative approach*. Elsevier, 2011.
- [16] Andrew G Howard, Menglong Zhu, Bo Chen, Dmitry Kalenichenko, Weijun Wang, Tobias Weyand, Marco Andreetto, and Hartwig Adam. MobileNets: Efficient convolutional neural networks for mobile vision applications. *arXiv preprint arXiv:1704.04861*, 2017.
- [17] Hengyuan Hu, Rui Peng, Yu-Wing Tai, and Chi-Keung Tang. Network trimming: A data-driven neuron pruning approach towards efficient deep architectures. *arXiv preprint arXiv:1607.03250*, 2016.
- [18] Weizhe Hua, Yuan Zhou, Christopher De Sa, Zhiru Zhang, and G Edward Suh. Boosting the performance of CNN accelerators with dynamic fine-grained channel gating. In *International Symposium on Microarchitecture (MICRO)*, pages 139–150. ACM, 2019.
- [19] Yuxiang Huan, Yifan Qin, Yantian You, Lirong Zheng, and Zhuo Zou. A multiplication reduction technique with near-zero approximation for embedded learning in IoT devices. In *International System-on-Chip Conference (SOCC)*, pages 102–107. IEEE, 2016.
- [20] Sergey Ioffe and Christian Szegedy. Batch normalization: Accelerating deep network training by reducing internal covariate shift. *International Conference on Machine Learning (ICML)*, 2015.
- [21] Cheolhwan Kim, Dongyeob Shin, Bohun Kim, and Jongsun Park. Mosaic-CNN: A combined two-step zero prediction approach to trade off accuracy and computation energy in convolutional neural networks. *Journal on Emerging and Selected Topics in Circuits and Systems*, 8(4):770–781, 2018.
- [22] Diederik P Kingma and Jimmy Ba. Adam: A method for stochastic optimization. *International Conference on Learning Representations (ICLR)*, 2014.
- [23] Alex Krizhevsky and Geoff Hinton. Convolutional deep belief networks on CIFAR-10. *Unpublished manuscript*, 40(7):1–9, 2010.
- [24] Alex Krizhevsky, Vinod Nair, and Geoffrey Hinton. CIFAR-10 and CIFAR-100 datasets. <http://www.cs.toronto.edu/~kriz/cifar.html>.
- [25] Alex Krizhevsky, Ilya Sutskever, and Geoffrey E Hinton. ImageNet classification with deep convolutional neural networks. In *Advances in Neural Information Processing Systems (NIPS)*, pages 1097–1105, 2012.
- [26] Sergey Levine, Chelsea Finn, Trevor Darrell, and Pieter Abbeel. End-to-end training of deep visuomotor policies.

- Journal of Machine Learning Research*, 17(1):1334–1373, 2016.
- [27] Guanpeng Li, Siva Kumar Sastry Hari, Michael Sullivan, Timothy Tsai, Karthik Pattabiraman, Joel Emer, and Stephen W Keckler. Understanding error propagation in deep learning neural network (DNN) accelerators and applications. In *International Conference for High Performance Computing, Networking, Storage and Analysis (SC)*, page 8. ACM, 2017.
- [28] Hao Li, Asim Kadav, Igor Durdanovic, Hanan Samet, and Hans Peter Graf. Pruning filters for efficient ConvNets. In *International Conference on Learning Representations (ICLR)*, 2017.
- [29] Ji Lin, Yongming Rao, Jiwen Lu, and Jie Zhou. Runtime neural pruning. In *Advances in Neural Information Processing Systems (NIPS)*, pages 2181–2191, 2017.
- [30] Yingyan Lin, Charbel Sakr, Yongjune Kim, and Naresh Shanbhag. PredictiveNet: An energy-efficient convolutional neural network via zero prediction. In *International Symposium on Circuits and Systems (ISCAS)*, pages 1–4. IEEE, 2017.
- [31] Jian-Hao Luo, Jianxin Wu, and Weiyao Lin. ThiNet: A filter level pruning method for deep neural network compression. In *International Conference on Computer Vision (ICCV)*, pages 5058–5066. IEEE, 2017.
- [32] Mostafa Mahmoud, Kevin Siu, and Andreas Moshovos. Diffy: a déjà vu-free differential deep neural network accelerator. In *International Symposium on Microarchitecture (MICRO)*, pages 134–147. IEEE, 2018.
- [33] Vinod Nair and Geoffrey E Hinton. Rectified linear units improve restricted boltzmann machines. In *International Conference on Machine Learning (ICML)*, pages 807–814, 2010.
- [34] Angshuman Parashar, Minsoo Rhu, Anurag Mukkara, Antonio Puglielli, Rangharajan Venkatesan, Brucek Khailany, Joel Emer, Stephen W Keckler, and William J Dally. SCNN: An accelerator for compressed-sparse convolutional neural networks. In *International Symposium on Computer Architecture (ISCA)*, pages 27–40. IEEE, 2017.
- [35] Ning Qian. On the momentum term in gradient descent learning algorithms. *Neural Networks*, 12(1):145–151, 1999.
- [36] Olga Russakovsky, Jia Deng, Hao Su, Jonathan Krause, Sanjeev Satheesh, Sean Ma, Zhiheng Huang, Andrej Karpathy, Aditya Khosla, Michael Bernstein, et al. ImageNet large scale visual recognition challenge. *International Journal of Computer Vision (IJCV)*, 115(3):211–252, 2015.
- [37] Tara N Sainath, Abdel-rahman Mohamed, Brian Kingsbury, and Bhuvana Ramabhadran. Deep convolutional neural networks for LVCSR. In *International Conference on Acoustics, Speech and Signal Processing (ICASSP)*, pages 8614–8618. IEEE, 2013.
- [38] Gil Shomron, Tal Horowitz, and Uri Weiser. SMT-SA: Simultaneous multithreading in systolic arrays. *Computer Architecture Letters (CAL)*, 18(2):99–102, 2019.
- [39] Gil Shomron and Uri Weiser. Spatial correlation and value prediction in convolutional neural networks. *Computer Architecture Letters (CAL)*, 18(1):10–13, 2019.
- [40] David Silver, Aja Huang, Chris J Maddison, Arthur Guez, Laurent Sifre, George Van Den Driessche, Julian Schrittwieser, Ioannis Antonoglou, Veda Panneershelvam, Marc Lanctot, et al. Mastering the game of Go with deep neural networks and tree search. *Nature*, 529(7587):484, 2016.
- [41] Karen Simonyan and Andrew Zisserman. Very deep convolutional networks for large-scale image recognition. *International Conference on Machine Learning (ICML)*, 2015.
- [42] Mingcong Song, Jiechen Zhao, Yang Hu, Jiaqi Zhang, and Tao Li. Prediction based execution on deep neural networks. In *International Symposium on Computer Architecture (ISCA)*, pages 752–763. IEEE, 2018.
- [43] Vivienne Sze, Yu-Hsin Chen, Tien-Ju Yang, and Joel S Emer. Efficient processing of deep neural networks: A tutorial and survey. *Proceedings of the IEEE*, 105(12):2295–2329, 2017.
- [44] Reza Yazdani, Marc Riera, Jose-Maria Arnau, and Antonio González. The dark side of DNN pruning. In *International Symposium on Computer Architecture (ISCA)*, pages 790–801. IEEE, 2018.
- [45] Jingyang Zhu, Jingbo Jiang, Xizi Chen, and Chi-Ying Tsui. Sparsenn: An energy-efficient neural network accelerator exploiting input and output sparsity. In *Design, Automation and Test in Europe Conference (DATE)*, pages 241–244. IEEE, 2018.